Secondary Structure Conformations and Long Range Electronic Interactions in Oligopeptides

John Wolfgang and Steven M. Risser*

Department of Physics, Texas A&M University−Commerce, Commerce, Texas 75429

Satyam Priyadarshy and David N. Beratan

Department of Chemistry, University of Pittsburgh, Pittsburgh, Pennsylvania 15260

Received: November 12, 1996[⊗]

Combined quantum mechanical coupling calculations and molecular dynamics simulations were performed to examine the role of modest geometrical fluctuations of peptide secondary structures on long range electronic interactions in oligopeptides. Molecular dynamics simulations were performed to obtain typical relevant conformations of oligopeptides, and self-consistent Hartree−Fock calculations at the semiempirical quantum theory level were performed to extract the long range electronic propagation. Initial α-helical oligopeptides show dominant hole-mediated coupling over a large tunneling energy range, while the initial extended conformation oligopeptides have more nearly equal contributions from both hole and electron mechanisms. Modest geometrical fluctuations lead to changes in the character of long range electronic interactions. The computations highlight the danger of drawing conclusions from electronic structure calculations of electronic coupling in peptide model systems on the basis of computations on single geometries.

Introduction

Considerable recent progress has been made in understanding how macromolecule structure controls long range electron transfer (ET) rates.[1] In the weak coupling limit, the ET rate is proportional to the donor−acceptor electronic coupling (T_{DA}) and the nuclear Franck−Condon factor (FC)[2]

$$k_{ET} = \frac{2\pi}{\hbar}|T_{DA}|^2\,(FC) \tag{1}$$

In the last 10 years, a significant effort focused on determining the dependence of T_{DA} on the structure of the chemical[3] or biochemical[4] bridge between donor and acceptor. *Pathways*[5] and related empirical methods provide an understanding of structural effects on ET rates in numerous proteins. However, more detailed questions associated with quantum interference between pathways, protein dynamics, and electron vs hole contributions to the long range mediation of the coupling are still open. In this paper, we describe a study based upon self-consistent field Hartree−Fock calculations that examines the role of structural fluctuation on the magnitude and mechanism of coupling in peptides with α-helix and extended motifs. We show that considerable changes in the magnitude and mechanism of coupling may arise with modest geometric changes. This study suggests that quantum chemical computations of protein-mediated electronic coupling need to consider an ensemble average of conformations in order to make quantitative predictions and mechanistic interpretations.

Computational Methods

The electronic coupling matrix element between donor and acceptor, T_{DA}, is

$$T_{DA} = \mathbf{V}_{DB}\mathbf{G}_{BB}\mathbf{V}_{BA} \tag{2}$$

within a two-level approximation when an orthogonal basis is employed.[6] Here **G** is the Green's function matrix of the bridge, which is[7]

$$\mathbf{G} = (E\,\mathbf{I} - \mathbf{H})^{-1} \tag{3}$$

H is the Hamiltonian of the bridge, **I** is the identity matrix, and E is the tunneling energy (**V** couples D and A to bridge). The Hamiltonian of the bridge incorporates the effect of protein structure and its propensity to mediate tunneling via its filled and empty orbitals. Changes in the three-dimensional structure of the bridge influence both **H** and **G**. The calculations here are based on the complete neglect of differential overlap (CNDO) level of quantum theory[8] with the CNDO/S parameterization.[9] Thus the self-consistent Fock matrix is used to obtain **G**. Larsson and others[10] have used this approach to interpret and to predict long range electron transfer rates in small molecules and biomolecules. Newton and co-workers[11] used a refinement of this method to describe small molecule ET. The Hartree−Fock−Roothan equations developed in the CNDO approximation have a unit overlap matrix,[8] which avoids complications arising in other methods.[12]

Within the Hartree−Fock approximation, the elements of **G** between bridge atomic orbitals i and j are[13]

$$\mathbf{G}_{ij} = \sum_m \frac{\langle i|m\rangle\langle m|j\rangle}{E - E_m} + \sum_n \frac{\langle i|n\rangle\langle n|j\rangle}{E - E_n} \tag{4}$$

where $|m\rangle$ are the states of the $N-1$ electron bridge (hole states) and $|n\rangle$ are the $N+1$ electron states (electron states) of the bridge. E_m is the energy of the mth bridge molecular orbital. This separation into sums over occupied and unoccupied orbitals allows analysis of T_{DA} in terms of electron- and hole-mediated components

$$T_{DA} = T_{DA}^{(elec)} + T_{DA}^{(hole)} \tag{5}$$

In the Hartree−Fock approximation[10a,13] the hole and electron states are derived from molecular orbitals of the bridge, so[14]

[⊗] Abstract published in *Advance ACS Abstracts,* February 15, 1997.

S1089-5647(96)03771-6 CCC: $14.00

$$T_{DA}^{(elec)} = \sum_{n(unocc)} \sum_{ik} \frac{\nu_{Di} C_i^n C_k^n \nu_{kA}}{E_n - E}$$

$$T_{DA}^{(hole)} = \sum_{m(occ)} \sum_{ik} \frac{\nu_{Di} C_i^m C_k^m \nu_{kA}}{E_m - E} \quad (6)$$

Here, D and A correspond to the donor and acceptor orbitals and *i* and *k* are all bridge atomic orbitals coupled to the donor or acceptor, respectively. $\nu_{Di(kA)}$ is the interaction matrix element between atomic orbital *i(k)* of the bridge and the D(A) orbital of the redox species. The donor/acceptor orbitals may, themselves, consist of multiple atomic orbitals. In the calculations reported here, we present the Green's function element between pairs of hybrid sp^3 orbitals located on the second and next-to-last C_α's of the oligopeptide in a well-defined secondary structure.

Oligoalanine α-helices 21 amino acids in length, and extended strands 15 residues in length, were constructed using the default angles in Macromodel. Energy minimization was then performed to reduce the steric interactions within the side chains with the peptide backbone atomic coordinates frozen. Molecular dynamics (MD) simulations were performed on these structures to generate alternative conformations with modest changes in structure. The simulations used the OPLS force field,[15] and solvent was included within the GB/SA continuum model.[16] The MD simulations were run for 15 ps with 1.5 fs time steps at a temperature of 300 K,[17] with the structural data saved every 0.15 ps. The 15 central residues were then taken from the α-helix and terminated to provide an α-helix of 15 residues in length. Geometries with less than 1.0 Å root-mean-square (rms) deviation of all atoms[18] from the initial structure were accepted and used in the following quantum calculations. The α-helix structures also had to satisfy the condition that none of the hydrogen bonds along the helix be longer than 3.00 Å.

Results and Discussion

CNDO/S calculated IP's and EA's provide close agreement with known experimental values and are in reasonable agreement with *ab initio* calculations for amino acids.[10,19] This is of great importance because these energies enter the denominators in the sum on states expression (eq 4−6). While many previous calculations on peptides and proteins used the extended-Huckel method,[20] they lead to an energy gap more relevant to *N*-electron photoexcitation processes than to the $N \pm 1$ electron virtual states that mediate ET. For the oligoalanine studied here, the HOMO energy occurs in the range −9.0 to −11.0 eV, while the LUMO is near 0 eV. These energies differ somewhat for the α-helix and extended structures and also vary from conformation to conformation within each motif. The tunneling energy relevant for typical biological donors and acceptors lies near the middle of this HOMO−LUMO gap, ∼5−6 eV binding energy,[10c,21,22] and can be tuned by changing the donor and acceptor structure.[23] The present analysis does not restrict itself to a single tunneling energy but reports the Green's function between the pair of C_α sp^3 orbitals for the range of tunneling energy from −8.0 to 0.0 eV, with energy increments of 0.05 eV.

Figure 1 shows the energy dependence of the hybridized Green's function element (propagation) for ALA_{15} in the initial α-helical conformation (**A0**), along with the decomposition into electron and hole components. The structure of **A0** is shown in Figure 2. The propagation is a smooth function of tunneling energy, with the propagation nearly energy independent near the middle of the range (most relevant for biological ET). The electron and hole components here have the same sign, leading to constructive interference between the two tunneling mechanisms. The energy where the electron and hole contributions are equal (∼−2.3 eV) defines the transition from primarily hole mediation to electron mediation. The fact that this transition point is asymmetric with respect to the center of HOMO−LUMO gap has been noted in hydrocarbon spacers and arises from the interferences associated with electron mediation pathways.[24]

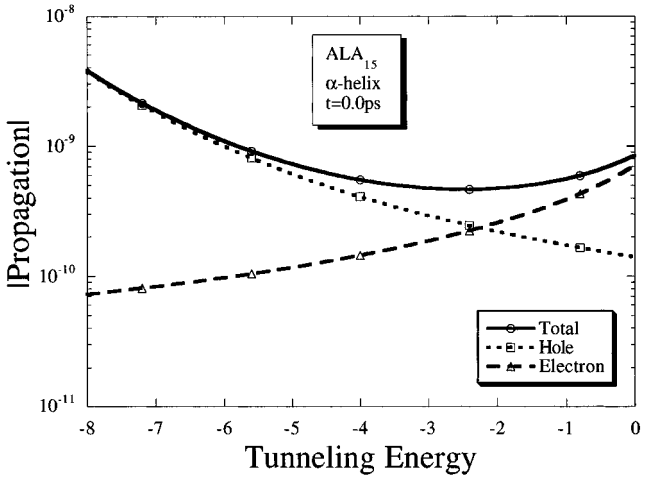

Figure 1. Total (solid line), electron (dashed line), and hole (dotted line) propagation between the 2nd and 14th amino acids, as a function of tunneling energy for the initial α-helical oligoalanine, **A0**. Propagation is in units of eV^{-1}, and tunneling energy is in units of eV.

The propagation in the original extended conformation (**B0**) appears in Figure 3, with the structure of **B0** shown in Figure 2. In this structure, the propagation exhibits more complex behavior, including a sign change in the propagation near −6.8 eV. This energy is far from the frontier orbitals of this system, which lie at −11.59 and +2.50 eV. The propagation at energies above this node shows weak energy dependence. This node in the propagation amplitude arises from a sign change in the hole-mediated propagation near −6.8 eV. The node in the hole-mediated propagation can be attributed to interferences between competing hole-mediated tunneling pathways. The electron contribution, in contrast, increases monotonically across this energy range.

The Green's function between the 2nd and 14th amino acids for the extended conformation is several orders of magnitude smaller than that found for the α-helix at all tunneling energies. This difference in the magnitude of the propagation cannot be attributed solely to the much larger separation distance between the donor and acceptor orbitals in the extended conformation (43.8 Å) than in the α-helix (19.0 Å), because there is an equal number of covalent bonds linking the donor and acceptor in both conformations. Instead, the difference in coupling between the two conformations can be attributed to the different set of non-nearest-neighbor interactions present in the conformations.

The extended conformations and α-helices also exhibit dramatically different distance decay rates for the propagation. The propagation between sp^3 hybrid orbital pairs on all the α-carbons has been calculated and used to determine the average distance decay of the coupling fit to the approximate formula

$$T_{DA} \propto \exp\left[-\frac{\beta}{2} R_{DA}\right] \quad (7)$$

Fits were obtained from the propagations between the 2nd residue and the 4th to 14th residues, at a tunneling energy of

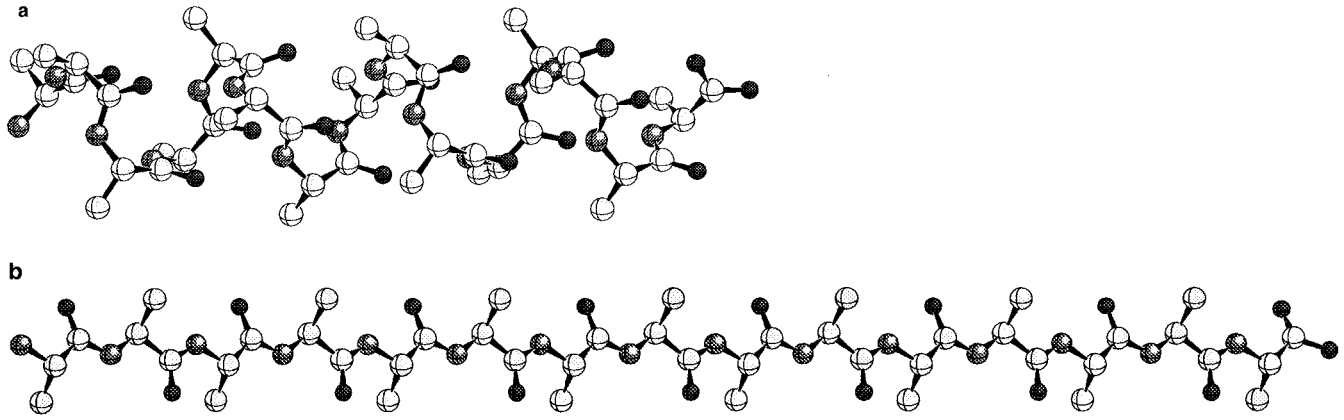

Figure 2. Initial conformations used in the Green's function calculations: (a) initial α-helix, **A0**; (b) initial extended conformation **B0**. Shown are all the heavy atoms of the structures. Carbon atoms are white, oxygen atoms are black, and nitrogen atoms are gray.

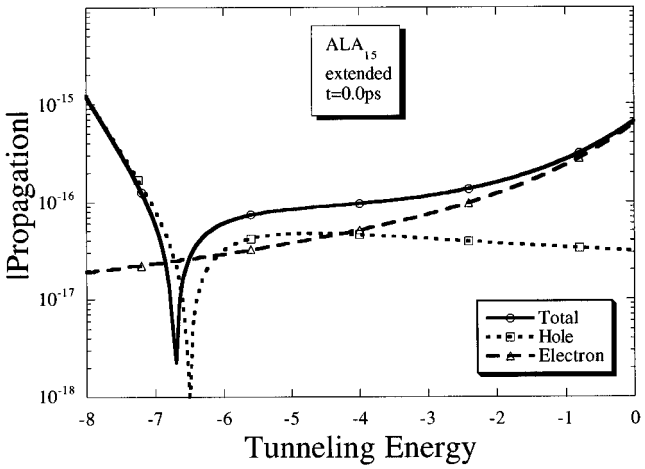

Figure 3. Total (solid line), hole (dotted line), and electron (dashed line) components of the propagation between the 2nd and 14th amino acids, as a function of tunneling energy for oligoalanine in the initial extended conformation, **B0**. Propagation is in units of eV^{-1}, and tunneling energy is in units of eV.

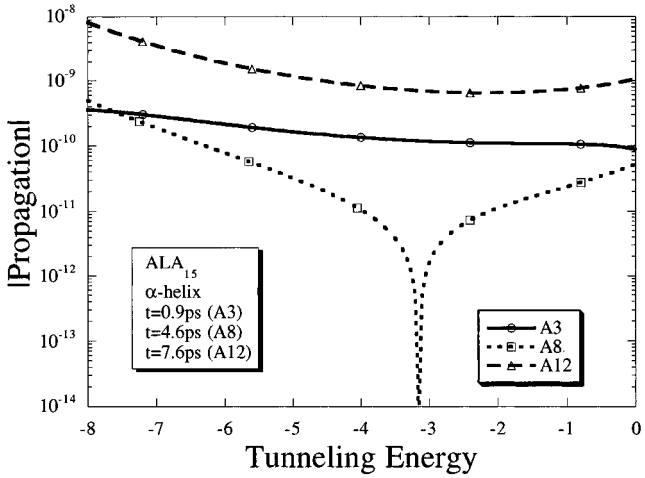

Figure 4. Total propagation as a function of tunneling energy for α-helix structures **A3** (solid line), **A8** (dotted line), and **A12** (dashed line). Structures were sampled from the MD simulation and have less than 1 Å rms deviation from the original structure.

−5.0 eV. This energy falls in the region where the coupling is essentially energy independent for the two conformations. The distance decay constant ($\beta/2$) for the initial extended conformation was computed to be 0.61 $Å^{-1}$. The distance decay rate for the initial α-helix was found to be 0.97 $Å^{-1}$. The larger value for the α-helix compared to the extended conformation is consistent with earlier predictions of *Pathway* analysis[5a] and with recent experiments.[25]

We can readily interpret these results in light of recent examinations of coupling in extended alkane chains, which suggested only nearest-neighbor and next-nearest-neighbor interactions are essential to describe the coupling.[24,26] These results[26a] also showed that nodes in the coupling as a function of energy could arise from competition between coupling pathways. We have examined how interatomic interactions within the peptides influence the coupling and found that in the α-helices interactions up to a cutoff distance of 3 Å must be included to properly describe the bridge-mediated coupling. This 3 Å cutoff incorporates nearest-neighbor and next-nearest-interactions between bonds, as well as the hydrogen-bonding interactions. The calculations for extended conformations are more sensitive to cutoff distances in the Hamiltonian matrix, and a cutoff of 3 Å artificially introduces an extra node in the propagation as a function of tunneling energy.

We examine the sensitivity of the propagation to relatively small changes in the α-helix geometry in Figure 4. The Green's functions for three alternate helix conformations, **A3**, **A8**, and **A12**, were calculated on the basis of conformations obtained from the MD simulation described above. The donor−acceptor attachment point separations for the conformations are given in Table 1, which shows the separation distance to have only small variation between the different conformations. The propagation in conformation **A3** appears similar (as a function of tunneling energy) to that of the starting conformation (**A0**). However, the propagation has *decreased* by 1 order of magnitude. Conformation **A8** has propagation that is smaller than in **A1**, but a node in the propagation has entered at an energy of ∼−3.2 eV. Although these examples suggest that propagation appears to decrease monotonically in time, the change in propagation is not "permanent". In conformation **A12**, the propagation is similar in shape and approximately twice the magnitude of the original conformation. The propagation in **A12** does not increase as rapidly at high energy as in **A0**, because of a decrease in the electron contribution to the propagation.

TABLE 1: Donor−Acceptor Separation for the α-Helix and Extended Conformations

	conformation	donor−acceptor distance (Å)
α-helix	**A0**	19.00
	A3	19.17
	A8	18.98
	A12	18.68
extended	**B0**	43.79
	B1	42.77
	B3	44.10
	B8	43.28

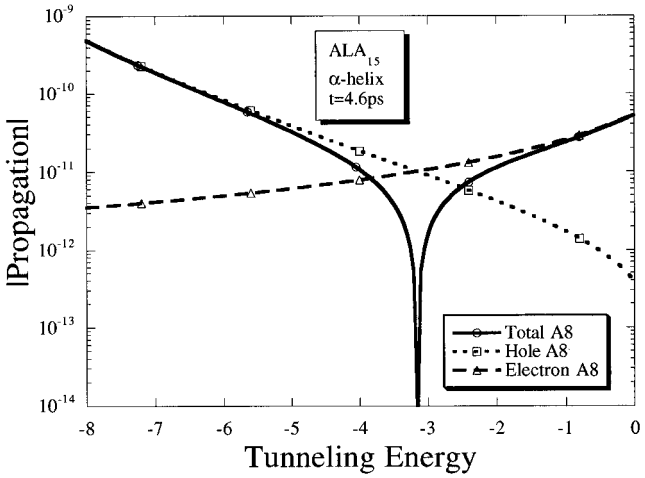

Figure 5. Total (solid line), hole (dotted line), and electron (dashed line) components of the propagation for α-helix structure **A8**.

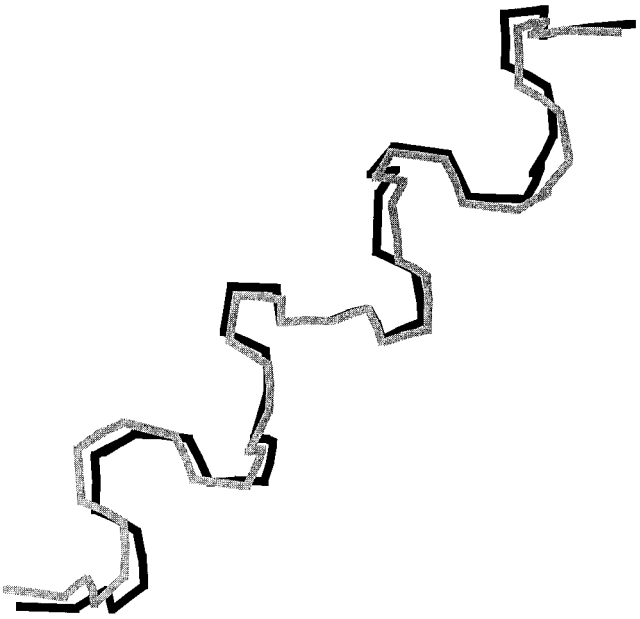

Figure 6. Overlay of the peptide backbone of conformations **A0** (dark line) and **A8** (light line).

The propagation in conformation **A8** is examined in more detail in Figure 5. Here, the node in the total propagation occurs because the hole and electron contributions are equal in magnitude but opposite in sign. This contrasts the original extended conformation, **B0**, where the node in the total propagation occurred because the dominating hole contribution itself underwent a sign change. The electron component of the propagation is similar to that computed in **A0** but is an order of magnitude smaller. The node in the total propagation marks where there is a crossover from a dominant hole mechanism to a dominant electron-mediated mechanism. This crossover occurs at an energy of −3.2 eV, lower than the crossover in the original conformation, which was hole dominated below an energy of −2.3 eV.

Although the magnitude of the total propagation varies greatly with conformation, the changes do not arise from drastic variations in the molecular geometry. The largest change in the propagation occurs in **A8**, where the propagation decreases by almost 2 orders of magnitude from that of **A0** and has a node. Figure 6 presents an overlay of the peptide backbones of **A0** and **A8**. Comparison of the two helices shows little difference between the two, other than some slight coiling and

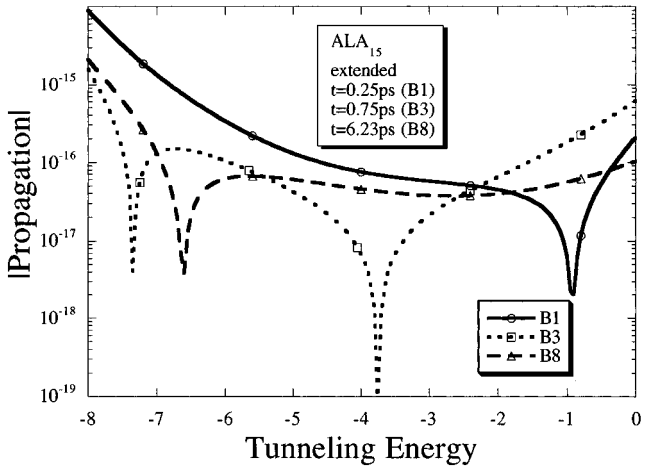

Figure 7. Total propagation as a function of tunneling energy for extended structures **B1** (solid line), **B3** (dotted line), and **B8** (dashed line). Structures were sampled from the MD simulation and have less than 1 Å rms deviation from the original structure.

uncoiling of backbone, reflected in hydrogen bond distance changes. These changes in the propagation also cannot be attributed dominantly to side chain geometry. Calculations performed on oligoglycine helices show very similar fluctuations, as do preliminary calculations on other homopeptide helices. The propensity for the magnitude and the sign of the hole and electron components of the propagation to fluctuate seems to be an intrinsic property of the α-helices studied. The fluctuations seem to be tied to the changes in the hydrogen bond structure.

Figure 7 shows how small changes in structure influence the propagation in extended peptides (structures **B1**, **B3**, and **B8**). The propagation in **B1** is larger at low energies than in the original conformation, and the node near −7.0 eV has disappeared. However, **B1** has a new node in the propagation near −1.0 eV, the origin of which is discussed below. The propagation in **B3** has two unique nodes at −7.5 and −3.8 eV and has decreased in magnitude from that of **B1**. **B8** re-exhibits propagation similar to that in the original conformation, with the node in the propagation shifted to a slightly lower tunneling energy and a smaller increase in the propagation near the top of the energy range.

Although the propagation in B3 deviates substantially from that computed in the original structure **B0**, this change does not arise from gross distortions of the structure. The most significant change in the propagation occurs in **B3**, where a second node in the coupling appears. Comparison of **B3** with the original structure shows that the heavy atoms have an rms deviation in their positions of only 0.68 Å and an rms deviation for all atoms of 0.87 Å. Examination of the peptide backbone of **B3** shows that there is slight distortion of the structure from planarity, but the changes from the **B0** backbone are smaller than could be resolved from an overlay plot. The propagation is almost the same in the **B8** conformation as in the original, despite geometric differences. The rms deviation of heavy atoms between the two conformations is 0.69 Å, with the rms deviation for all atoms 0.87 Å. Thus, the larger change in the **B8** geometry actually produce much smaller changes in the total propagation than in the **B3**.

Figure 8 shows the electron and hole propagation in **B3** in greater detail. The two nodes in the coupling arise for two distinct reasons. The low-energy node is caused by a node in the hole-mediated propagation, a result of destructive interference between competing hole-mediated pathways. This node occurs far from the HOMO energy, which has risen in this

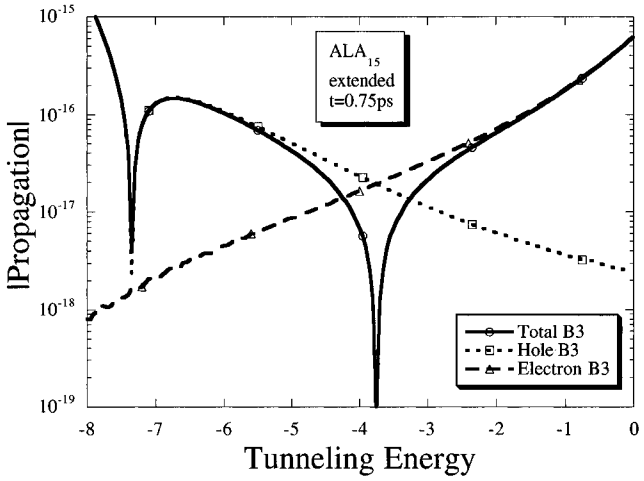

Figure 8. Total (solid line), hole (dotted line), and electron (dashed line) components of the propagation for extended structure **B3**.

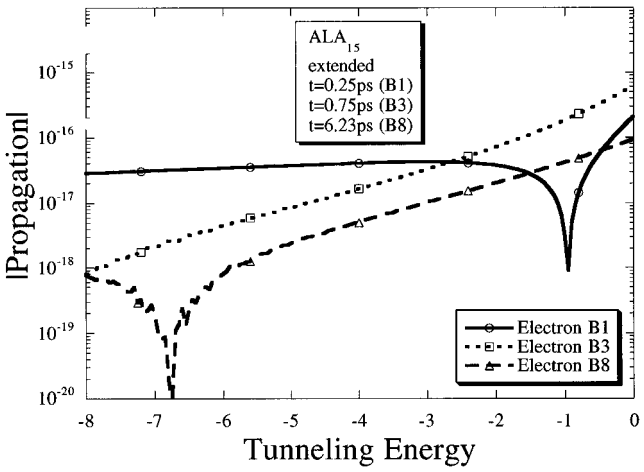

Figure 9. Electron-mediated propagation as a function of tunneling energy for extended structures **B1** (solid line), **B3** (dotted line), and **B8** (dashed line). Structures were sampled from the MD simulation and have less than 1 Å rms deviation from the original structure.

conformation to −11.38 eV and was −11.59 eV in the original conformation. At no time did the HOMO or LUMO in any of the structures approach the tunneling energy range being probed. The node near the center of the HOMO/LUMO gap arises from cancellation between the hole and electron components. The electron contribution to the propagation in this conformation is similar to that in the original conformation.

All of the electron propagation components examined here in the α-helix and extended conformations have been similar in appearance, with a monotonic increase in propagation as the tunneling energy increases. This pattern, though common, is not universal. Figure 9 shows the electron component of the coupling for the three extended conformations of Figure 7. In two of the conformations (**B1** and **B8**) the electron-mediated component has a node. In **B8**, the node occurs at an energy where the hole-mediated coupling dominates, and so the electron-mediated coupling does not alter the total coupling. In **B1**, the node in the electron-mediated coupling occurs for an energy where the electron propagation is dominating, thus giving rise to the node in the total coupling seen in Figure 7.

Conclusions

Coupled quantum mechanical calculations and molecular dynamics simulations present protein-mediated long range electronic couplings that change in magnitude and sign with the changes in the conformation fluctuations of the bridge. When these fluctuations are rapid compared to electron transfer reactions "decision times", the mean square value of the coupling should enter the rate.[27] While average secondary structure effects calculated here are qualitatively consistent with simple models, the dominance of the electron- vs hole-mediated coupling components and the magnitude of the coupling fluctuations are not apparent in single-geometry calculations. α-helical oligoalanine showed a prominence of the hole contribution in the original conformation, while the original extended oligoalanine showed electron mediation to dominate. For both structures the electron and hole propagation is sensitive to the conformation changes of the oligopeptides. Observed rates of ET not only reflect the averages over structures analyzed here but also depend upon how the donor and acceptor "integrate" wave function amplitude. Increased attention to detailed protein structural fluctuations, and to appropriate averaging of couplings, is essential for meaningful detailed comparisons between theory and experiment. The kinds of fluctuations examined here will be of great importance for interpreting ET in model peptides.[28] Related studies in more highly constrained proteins are also of great current interest.

Acknowledgment. This work is supported by a Cottrell College Science Award of the Research Corporation, Department of Energy (DE-FG36-94G010051), the National Science Foundation (CHE-9257093), and East Texas State University. Support of this work through Cray Research grants at the Pittsburgh and San Diego Supercomputing Center is gratefully acknowledged.

References and Notes

(1) (a) Bendall, D. S. *Protein Electron Transfer*; BIOS Scientific Publishers: Oxford, 1996. (b) Sigel, H.; Sigel, A. *Metals Ions in Biological Systems*; Marcel Dekker Press: New York, 1992. (c) Beratan, D. N.; Betts, J. N.; Onuchic, J. N. *Science* **1991**, *252*, 1285. (d) Onuchic, J. N.; Beratan, D. N.; Winkler, J. R.; Gray, H. B. *Annu. Rev. Biophys. Biomol. Struct.* **1992**, *21*, 349.

(2) Marcus, R. A.; Sutin, N. *Biochim. Biophys.* **1984**, *811*, 265 and references therein.

(3) (a) Casimiro, D. R.; Richards, J. H.; Winkler, J. R.; Gray, H. B. *J. Phys. Chem.* **1993**, *97*, 13073. (b) Farver, O.; Pecht, I. *Biophys. Chem.* **1994**, *50*, 203. (c) Cheng, J.; Saghi-Szabo, G.; Tossell, J. A.; Miller, C. *J. Am. Chem. Soc.* **1996**, *118*, 680.

(4) (a) Bertini, I.; Gray, H. B.; Lippard, S. J.; Valentine, J. S. *Bioinorganic Chemistry*; University Science Books: Mill Valley, CA, 1994. (b) Meade, T. J. In *Metal Ions in Biological Systems*; Marcel Dekker Press: New York, 1996; Vol. 32, p 453.

(5) (a) Beratan, D. N.; Betts, J. N.; Onuchic, J. N. *Science* **1991**, *252*, 1285. (b) Onuchic, J. N.; Beratan, D. N. *J. Chem. Phys.* **1990**, *92*, 722.

(6) Larsson, S. *J. Am. Chem. Soc.* **1981**, *103*, 4034 and references therein.

(7) Economou, E. N. *Green's Function in Quantum Physics*; Springer Verlag: New York, 1990.

(8) Pople, J. A.; Beveridge, D. L. *Approximate Molecular Orbital Theory*; McGraw Hill: New York, 1970.

(9) Del Bene, J.; Jaffe, H. H. *J. Chem. Phys.* **1968**, *48*, 1807.

(10) (a) Larsson, S.; Braga, M. *Int. J. Quantum Chem., Quantum Biol. Symp.* **1993**, *20*, 65. (b) Larsson, S.; Braga, M. *J. Phys. Chem.* **1993**, *97*, 8929. (c) Braga, M.; Larsson, S. *Int. J. Quantum Chem.* **1992**, *44*, 839. (d) Priyadarshy, S.; Risser, S. M.; Beratan, D. N. *Int. J. Quantum Chem., Quantum Bio. Symp.* **1996**, *23*, 65. (e) Priyadarshy, S.; Risser, S. M.; Beratan, D. N. *J. Phys. Chem.* **1996**, *100*, 17678.

(11) Newton, M. D. Chem. Rev. **1991**, *91*, 767; *J. Phys. Chem.* **1992**, *92*, 3049.

(12) Priyadarshy, S.; Skourtis, S. S.; Risser, S. M.; Beratan, D. N. *J. Chem. Phys.* **1996**, *104*, 9473.

(13) Szabo, A.; Ostlund, N. *Modern Quantum Chemistry: Introduction to Advanced Electronic Structure Theory*; Macmillian: New York, 1982.

(14) (a) Hale, P. D.; Ratner, M. A. *Int. J. Quantum Chem.* **1984**, *S18*, 195. (b) Richardson, D. E.; Taube, H. *J. Am. Chem. Soc.* **1983**, *105*, 40.

(15) Jorgensen, W. L.; Tirado-Rives, J. *J. Am. Chem. Soc.* **1988**, *110*, 1657.

(16) Still, W. C.; Tempczyk, A.; Hawley, R. C.; Hendrickson, T. *J. Am. Chem. Soc.* **1990**, *112*, 6127.
(17) Fraga, S.; Parker, J. M. R.; Pocock, J. M. *Computer Simulations of Protein Structures and Interactions*; Springer: Berlin, 1995.
(18) Root-mean-square deviations were calculated as deviation $({}^{1}/_{N} \sum_i |\mathbf{r}_i - \mathbf{r}'_i|^2)^{1/2}$, where $\mathbf{r}_i$ are the initial coordinates and $\mathbf{r}'_i$ are the new coordinates, both measured from the center of mass of the peptide.
(19) Colson, A.-O.; Besler, B.; Close, D. M.; Sevilla, M. D. *J. Phys. Chem.* **1992**, *96*, 661.
(20) Hoffmann, R. *J. Chem. Phys.* **1963**, *39*, 1397; **1964**, *40*, 2474, 2745.
(21) Gruschus, J. M.; Kuki, A. M. *J. Phys. Chem.* **1993**, *97*, 5581.
(22) Felts, A. K.; Pollard, W. T.; Friesner, R. A. *J. Phys. Chem.* **1995**, *99*, 2929.
(23) Beratan, D. N.; Onuchic, J. N.; Hopfield, J. J. *J. Chem. Phys.* **1987**, *86*, 4488.
(24) Jordan, K. D.; Paddon-Row, M. N. *Chem. Rev.* **1992**, *92*, 395.
(25) Langen, R.; Chang, I-J.; Germanas, J. P.; Richards, J. H.; Winkler, J. R.; Gray, H. B. *Science* **1995**, *268*, 1733.
(26) (a) Balabin, I.; Onuchic, J. N. *J. Phys. Chem.* **1996**, *100*, 11573. (b) Newton, M. D. *Chem. Rev.* **1991**, *91*, 767. (c) Naleway, C. A.; Curtiss, L. A.; Miller, J. R. *J. Phys. Chem.* **1991**, *95*, 8434.
(27) Onuchic, J. N.; Wolynes, P. G. *J. Phys. Chem.* **1988**, *92*, 6495.
(28) (a) Isied, S. S.; Ogawa, M. Y.; Wishart, J. F. *Chem. Rev.* **1992**, *92*, 381. (b) Gretchikhine, A.; Deguzman, K.; Ogawa, M. Y. *J. Am. Chem. Soc.* **1996**, *118*, 1543. (c) Dahiyat, B. I.; Meade, T. J.; Mayo, S. L. *Inorg. Chim. Acta* **1996**, *243*, 207.